BER the international journal of bridge engineering management and research

Timber Bridge Pile Splicing with Traditional and Fiber-Reinforced Polymer Wrap Methods

GangaRao Hota[1,*]; Drew Damich[1]; Walid Alaywan[2,3]; V. J. Gopu[2,3] and Chao Zhang[1]

Submitted: 23 February 2026 **Accepted:** 26 March 2026 **Publication date:** 10 April 2026

DOI: 10.70465/ber.v3i2.82

Abstract: Current timber pile splicing mechanisms utilize various steel, concrete, or wooden components. This study evaluated the strength capacities of steel and wood splicing mechanisms in addition to the fiber-reinforced polymer (FRP) wrap splice mechanism. Splicing mechanisms studied herein are flat steel plate, C-channel steel plate, wooden plate splices, and FRP wrap splices, consisting of unidirectional glass/epoxy composite with three and six layers of glass fabrics, which were reinforcing wooden components in both the longitudinal and hoop directions. These four splicing mechanisms were tested and compared under shear, bending, and axial loads. Of the three traditional splicing mechanisms (excluding FRP wrap), the C-channel was the strongest for each loading scenario except for axial loading. The FRP wrap method was the strongest under axial loading; it lacked in bending capacity compared to other methods. Bending failure in FRP splicing mechanism occurred due to the lack of adequate fiber reinforcement in the hoop direction of the timber pile. To improve the bending and shear capacity of FRP-spliced pile along the hoop direction, a six-layer fabric architecture was adopted, which showed significant improvement in bending and shear capacities from the original three-layer glass FRP composite wrap design. Even though the bending failure capacity of FRP-wrapped composite with six layers is slightly lower (∼15%) than the bending capacity of pile repaired with traditional splice mechanisms, axial and shear capacities of FRP-spliced system were higher than those from traditional methods. With increases in the number of wrap layers and FRP fabric density, even bending capacity can be improved, and the deformation is far less than the deformation of wood piles with traditional splice mechanisms.

Author keywords: Timber Piles; traditional splicing mechanisms; glass fiber–reinforced polymer composite wraps

Introduction

Timber bridge piles often require repair due to decay in areas of high moisture,[1] especially in the splash zones. After removing the decayed portions of timber piles, several different splicing mechanisms using wood or steel are being used in the field, with limited service life. Therefore, fiber-reinforced polymer (FRP) wrapping has been evaluated for splicing of timber piles not only to prevent decay but also to provide adequate strength to transfer forces to the ground.

West Virginia University-Constructed Facilities Center, jointly with Louisiana Transportation Research Center (LTRC), analyzed various splicing methods to repair deteriorated timber piles. Three traditional (legacy) splicing mechanisms (Figs. 1–3) and a newly developed FRP wrap splice (Fig. 4) mechanism were constructed and tested under various loading conditions. The three traditional splicing mechanisms tested in this program were flat steel plate, steel C-channel, and wooden plate. Each of the four splice designs was tested under shear, four-point bending, and axial compression to establish their load capacities. Test data were analyzed to determine the axial, bending, and shear stiffnesses and strengths of each splice design. The FRP wrap splice mechanism was further analyzed to develop the strength capacity equations.

Literature Review

Technical information available in the literature on traditional splicing was reviewed to arrive at better solutions using FRP composite wraps. The focus of the review was on resistances and service life of wood piles and FRP wrap systems under harsh environments.

Resistance of timber

According to Agricultural Handbook No. 557, timber bridge piles are susceptible to decay caused by fungi[1] due to aging,[2] moisture fluctuations (in splash zones), and temperature variations. Signs of fungal presence have been observed

*Corresponding Author: GangaRao Hota.
Email: hota.gangarao@mail.wvu.edu
[1]Department of Civil and Environmental Engineering, West Virginia University, Morgantown, WV 26506
[2]Department of Civil and Environmental Engineering, University of Louisiana at Lafayette, Lafayette, LA 70503, USA
[3]Louisiana Transportation Research Center, Louisiana Department of Transportation and Development, Baton Rouge, LA 70808, USA

Discussion period open till six months from the publication date. Please submit separate discussion for each individual paper. This paper is a part of the Vol. 3 of the International Journal of Bridge Engineering, Management and Research (© BER), ISSN 3065-0569.

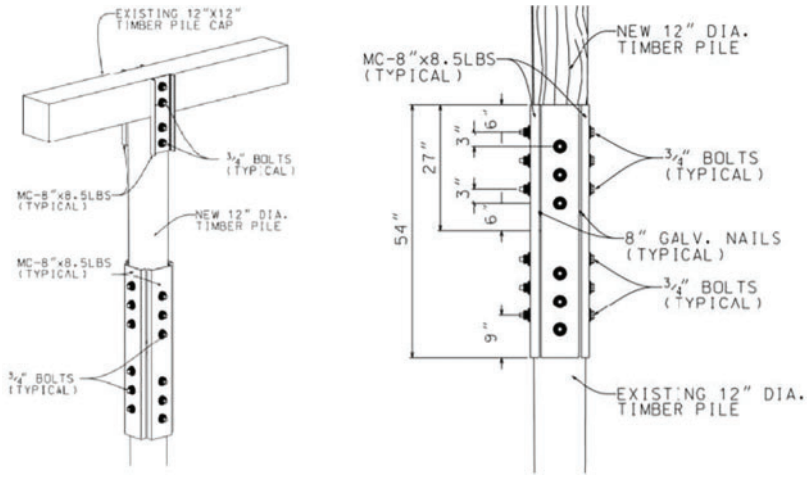

Figure 1. C-channel splice detail

Figure 2. Steel plate splice specimen

Figure 3. Shear test setup with wooden splice

Figure 4. Finished pile with glass fiber–reinforced polymer composite splice

such as softening of the wood, decrease in density, and discoloration.[3] The timber pile decay goes about 30 in. (762.0 mm) below the ground or mud line as the oxygen necessary for decay to occur decreases drastically with depth.[4] Bacteria can have decaying effects on wood. Unlike fungal deterioration, bacterial deterioration can occur under a wide range of conditions based on the species.[5] Insects such as termites are also known for their ability to feast on wood with high moisture content.[6,7] The natural fungal decay resistance in heartwood can range from highly resistant to zero resistance. Many timber bridges are classified as moderately resistant to decay but need preservative treatment for longer service life.[8] A variety of different preservatives have been used to prevent decay, with creosote, which is the most successful preservative for outdoor applications, but is banned for use in marine environments by some state governments in the United States. Other preservatives used to protect wood from environmental factors are available.[8] Inorganic salt-based preservatives such as Chromated Copper Arsenate (CCA) and Ammoniacal Copper Zinc Arsenate (ACZA) provide the disadvantage of lack of water repellency.[1] For this reason, oil-based preservatives like pentachlorophenol and creosote are mainly used in bridge members that are in contact with water.

Repair of timber pile

The repair methods discussed herein are splicing, supplemental piles, concrete jacketing, and FRP shells as wraps.

The method of splicing is often performed in situations where a pile needs to be accessed above ground; however, underwater repair of piles can be done with polymer composite wraps using polyurethane resin system that cures only under moisture exposure. Before splicing, typically, the structure is supported with a strut and jack, and the deteriorated portion is cut out and replaced with a section of similar diameter. The replaced timber section is secured using bolts to hold the separate pile sections together.[9] Additional details are shown in Figs. 1 to 3, which are similar to the ones shown by Dahlberg et al.[10] and Klaiber et al.[11] Supplemental piles are utilized for piles with severe deterioration, and this process can provide pile strengths exceeding the design strengths of existing members. Concrete jacketing is used to repair timber piles that have experienced 10–50% section loss due to deterioration.[11,12] FRP wrapping with polyvinyl chloride (PVC) wrap was utilized to protect piles with small (10–15%) section loss by the US Army and Air Force (Bridge Inspection, Maintenance, and Repair (TM 5-600/AFJPAM 32-1088), 1994). This method is cheaper than concrete jacketing. In addition, the PVC wrap method provides protection against abrasion.[11] FRP shells filled with grout are utilized to increase the pile strength. The FRP shell has fiber orientation in both the axial and hoop directions, increasing the axial and shear capacities of the pile,[9,11] and protecting piles from parasite attacks.

FRP systems

FRP systems primarily consist of fibers and resin. Fibers come in the form of fabrics of different densities that provide most of the strength to the system.[13,14] The resin acts as a matrix that primarily holds fibers together and transfers shear forces.[15] FRP systems may also have additives and fillers to modify various properties of the FRP system.[16] Primers may also be added to FRP systems to ensure a good bond between the fabric and timber substrate. Column confinement using FRP wrapping is implemented to increase bending stiffness[17] and axial strength capacity in timber columns, in a manner similar to that of concrete column confinement. To improve the strength and stiffness of timber columns, CFRP wrap was used[18] in six timber column specimens with different wrapping orientations, including toroidal, single helix, double helix, cross helix, and all helix. Tests were performed by Garcia et al.[17] on wooden pine beams using carbon and basalt fiber composite wraps with unidirectional and bidirectional fiber orientation, resulting in increased beam stiffness and structural capacity. Laboratory testing on glass fiber–reinforced polymer (GFRP) wrapping on timber railroad bridge beams and timber piles/bents[19] resulted in repairing four 80+-year-old, creosote-treated, timber bridge beams and piles that had been deemed deficient and removed from bridge structures. Each of these specimens was first tested to failure and then repaired using U-shaped GFRP wraps. All the repaired specimen tests yielded lower load capacity than the control specimens. This was expected as the beams underwent significant damage. The repaired specimens exhibited a recovery strength of 55%–60% of the control (bending) strength with 3 layers of GFRP wraps and showed a significant improvement in ductility.[19] One of the specimens showed an increase in shear modulus after the specimen was repaired with GFRP wrap. Overall, specimens performed well after being repaired with GFRP wraps.

Field implementation

Field installation procedures were identified through literature.[19–21,22] Repair of decayed timber pile portions was performed not as a splice but as an FRP system after filling decayed portions with putty. Additional details can be found in the references.[19–21]

Splice Design and Analysis

As part of this study, the effectiveness of the three traditional splicing methods (as suggested by LTRC) was evaluated by measuring the shear, bending, and axial strengths to failure and the corresponding deformations. In addition, splicing of the new pile section and the old (undamaged in service) pile section was done by wrapping with GFRP fabrics overlapping the new and old (undamaged) pile sections.

The following sections expand upon the strength and stiffness of timber pile repair using the above four different splicing methods.

Assembly of cut specimens

In this study, 36 creosote-treated southern pine piles of 12 in. (±1 in.) diameter were tested under axial, shear, and bending with four splice configurations, with three replications of each configuration (Table 1). Virgin piles were cut to the desired lengths of 5 ft (1.52 m), 8 ft (2.44 m), or 16 ft (4.88 m) for axial, shear, and bending tests, respectively. They were cut further at midspan for splicing, as specified by LTRC, and additional splicing details are shown in Figs. 1–3.

FRP composite repair consists of glass fabric and resin. A variety of commercially available fabrics and resin systems were used. The Sika system, a unidirectional glass fabric (Sika Hex 100 G with 0.092lb/in^3 (2547.0 kg/m^3)), and Sikadur Hex 300 (two-part epoxy resin) were used herein to splice the timber piles.

Assembly of FRP composite splicing

The piles were cut in half before splicing with FRP wraps. The cut sections were nailed together to prevent pile separation or movement during wrapping. Sheets of fabric were cut to 4 ft (1.22 m) in length, creating a rectangular sheet of fabric with dimensions 48 × 51 in. (1.22 × 1.30 m). The 51 in. (1.30 m) is the width of the glass fabric roll supplied by Sika. The contents of the resin (Part A and Part B) were mixed using an electric mixer for five minutes, and the pile surface was primed with low-viscosity resin (∼500 cps) and then saturated with the glass fabric before circumferentially hand-wrapping the pile with three or six layers of fabric.

Table 1. Pile splice configuration

		Splicing method used				
Test type	Pile length	Flat steel plate	C-channel plate	Wood plate	FRP wrapping	
Axial	5 ft (1.52 m)	3	3	3	3	
Shear	8 ft (2.44 m)	3	3	3	3	
Bending	16 ft (4.88 m)	3	3	3	3	
	Total:	9	9	9	9	**36**

Note: FRP, fiber-reinforced polymer.

The pile was primed by liberally brushing the primer (low-viscosity resin) onto the surface of the pile and subsequently preparing the fabric by rolling resin onto both sides of the fabric. Thus, the entire glass fabric was ensured to have resin saturation to minimize voids after curing of the resin. The wet fabrics were stapled at the ends and pressed to provide adequate bond to the primed wood surface, which is uneven in large timbers. While the fabric was wrapped around the pile, the resin-saturated fabric was wiped and pressed by hand to remove voids and ensure a tight, void-free wrap, as shown in Fig. 4. This process can be easily mechanized and adopted in the field using the vacuum-assisted resin transfer molding method.

Testing Methods and Setup

Shear test setup

The shear test was prepared by placing two concrete supports with a clear span of 4 ft 8 in. (1.42 m) apart. To induce a shear mode of failure, span-to-depth (l/d) ratio of a test specimen, ranging between 4 and 8, was maintained. However, l/d < 6 is recommended as per ASTM D198-15 [32]. The test span (4 ft 8 in.) for shear test resulted in a l/d of 4.67 for 12 in. (0.305 m) diameter specimen (Fig. 5).

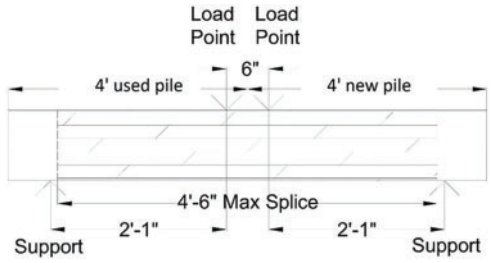

Figure 5. Shear test schematic (refer to Fig. 3)

An 8 ft (2.44 m) long pile was placed on steel saddles following the splicing at the center of the span of the refurbished pile (Fig. 3). The refurbished timber pile was loaded at the center using hydraulic actuator, with a load cell measuring the amount of force applied transversely onto the pile. Deflections were measured using linear variable differential transformer (LVDT) while applying the load.

Bending test setup

To obtain bending mode of failure, the span-to-depth (l/d) ratio was taken as 15. Therefore, the test specimen was spanned at 15 ft (4.57 m) between support saddles. A schematic of bending test setup is shown in Fig. 6. Other instrumentation remained the same as in the shear test setup. With the pile in position, an I-beam (Fig. 7) was placed on top of test specimens to distribute the load and create a test setup that generates a 4-point bending test. A string pot was used to measure the downward deflection under loading. All sensors were initialized (zeroed) before the I-beam was placed on the specimen.

Axial test setup

The axial compression test was performed by placing the 5 ft (1.52 m) long pile sections in a compression test frame, which had a load capacity of 750 kips, as shown in Fig. 9, while Fig. 8 shows the schematic of compression test setup. LVDTs were used to measure longitudinal displacement under compression.

Test Results and Data Analysis for Traditional (Legacy) Splicing

Data Analysis Under Shear Testing

Data were analyzed for maximum shear stress and deflection after plotting shear stress versus deflection. The maximum shear stress at depth d/2 of each test specimen is determined using classical Eqs. (1) and (2):

$$A = \frac{\pi d^2}{4} \tag{1}$$

$$\tau = \frac{4F}{3A} \tag{2}$$

where is d is the diameter of the pile cross section, A is the area of the pile cross section, τ is the shear stress, and F is the applied force.

For simplicity, shear stress was computed using the cross-sectional area at 3 different locations of each timber pile, neglecting the shear resistance offered by the splicing mechanism and the stress concentration induced by the holes drilled for splicing. Shear stress–displacement plots are

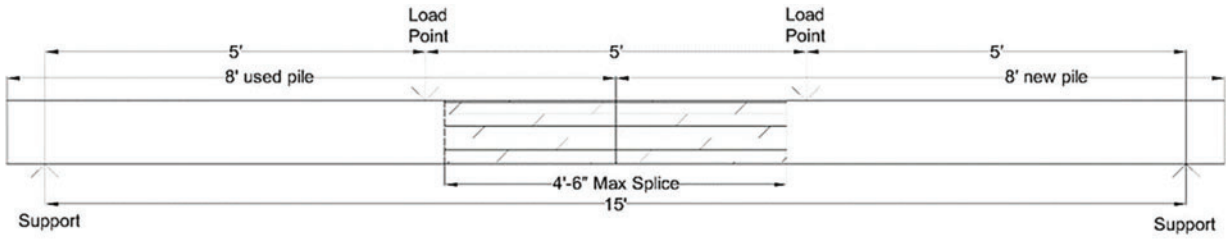

Figure 6. Flexural test schematic

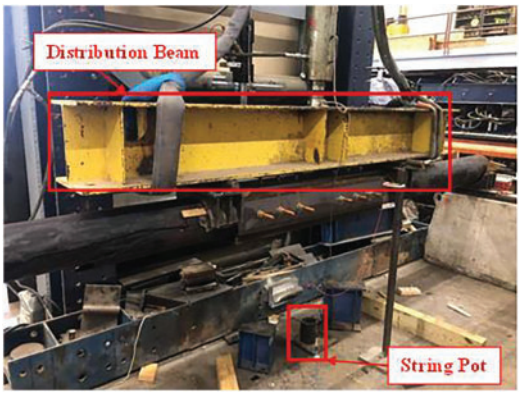

Figure 7. Flexure test setup with C-channel splice

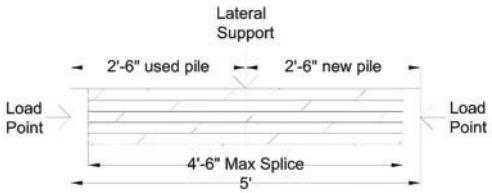

Figure 8. Axial compression test schematic

Figure 9. Axial test setup with C-channel splice

based on three replications of test specimens and are shown for each splice mechanism in Figs. 10–12.

Shear tests were performed on three 8-ft long piles, which were repaired using the three legacy repair methods, resulting in a total of nine tests (Table 1). Table 2 shows the maximum shear stress and the corresponding deflection for each of the nine test specimens, including their averages.

For clarity, we report average values for each configuration, while detailed statistical descriptors, including standard deviation and coefficient of variation, are provided in the Appendix. The variability of the results is considered in the comparative discussion.

Shear stress versus transverse deflection for timber piles spliced with flat steel plates is shown in Fig. 10. The test data revealed a 40% variation in shear stress (500 psi (3.45 MPa) versus 700 psi (4.83 MPa)), which is attributed to the quality of timber pile specimens, and such variation (~40%) is not unusual for large-diameter timbers. Random cracking was observed visually in timber piles and can be attributed to internal flaws in large-size timbers. It was observed that the first test exceeded the deflection measurement limit of the LVDT; hence, it was unable to record ultimate deflection.

Shear stress versus deflection for timber piles spliced with steel C-channel splicing is provided in Fig. 11. The test data revealed that the shear failure mode is nearly identical in all piles that were tested under shear failure mode. The C-channel method of splicing is found to be stronger than the steel plate splicing method. This is to be expected as the C-channel method provides higher shear resistance than the steel plate splice. Similar to the shear deflection response using steel plate, deflection peaked above the constraints of the test device (LVDT) for test one of this method. The initial slope change in Tests 1 and 2 of the steel plate splicing mechanism may be attributed to the initial internal adjustment of the test specimen at the early stages of loading. The C-channel splicing dug into the wooden pile upon initial loading. The load–deflection slope changes may also be a result of the yielding of steel at the load location, which was observed in multiple specimens that were repaired using this technique.

Fig. 12 provides the shear stress versus deflection plots for specimens with wooden plate splicing. The wooden plate splice, however, does not have the same yielding effect as the other two splicing methods. The wood splicing that was tested here was slightly weaker in shear than the other two.

In terms of shear strength of the piles based on the three legacy methods of splicing, the C-channel method was the strongest and the wood plate method was the weakest, with a 30% variation. The C-channel splice method provided higher shear resistance than the other two methods due to its large material volume and shape compared to the lesser volume of the flat steel plate splice. Under loading, the wooden splice plates interacted more in unison with the timber pile than the steel plates or C-channel splicing devices, which is attributed

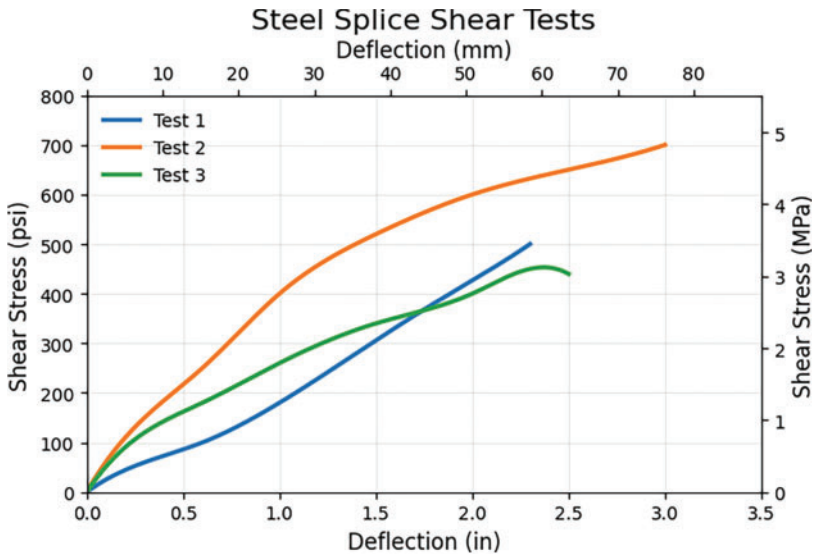

Figure 10. Shear stress versus deflection for steel plate splice

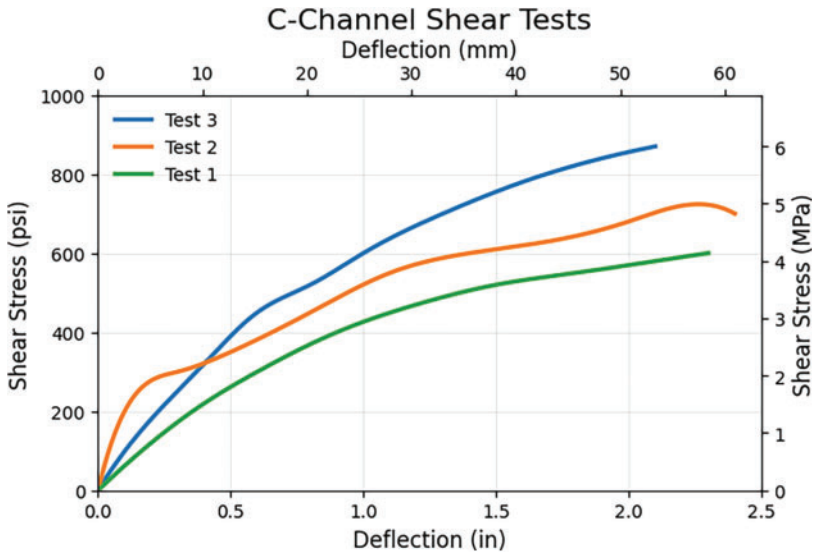

Figure 11. Shear stress versus deflection for C-channel splice

to better compatibility of modulus of the wood splicing mechanism and the timber pile. Wood splicing resulted in indentation from the applied load as well as cracking on the top and bottom wood plates.

Data analysis under bending

The test data under bending were analyzed to establish maximum bending stress (Eq. (3)) and deflection for circular cross sections

$$MOR = \frac{2Pa}{\pi r^3} \tag{3}$$

where MOR is the modulus of rupture, P is the applied load, a is the distance between the support and nearest point load, and r is the average radius test pile.

Table 3 shows the maximum bending stress (MOR) for 16 ft (4.88 m) span pile and the corresponding deflection.

A typical stress versus deflection (measured with string pot) using steel plate splicing mechanism is given in Fig. 13.

For timber piles spliced with the C-channel, three specimens were tested. The bending stress versus deflection data for the third test specimen could not be retrieved; hence, it was not included in Table 3 and Fig. 14. The large deviation in data of the two test samples (Fig. 14) was attributed to the original strength of the timber pile (before splicing) even though the failure behavior of the second test specimen was similar to that of the first one.

Fig. 15 reveals the bending versus deflection response of specimens spliced with wood. No significant change in bending versus deflection to failure was noted. It reveals that the splicing system causes the pile to split at failure, and not yield as observed in steel-plate or C-channel splicing.

A simplified section-property comparison indicates that the C-channel configuration provides substantially higher flexural stiffness and section modulus than the flat steel

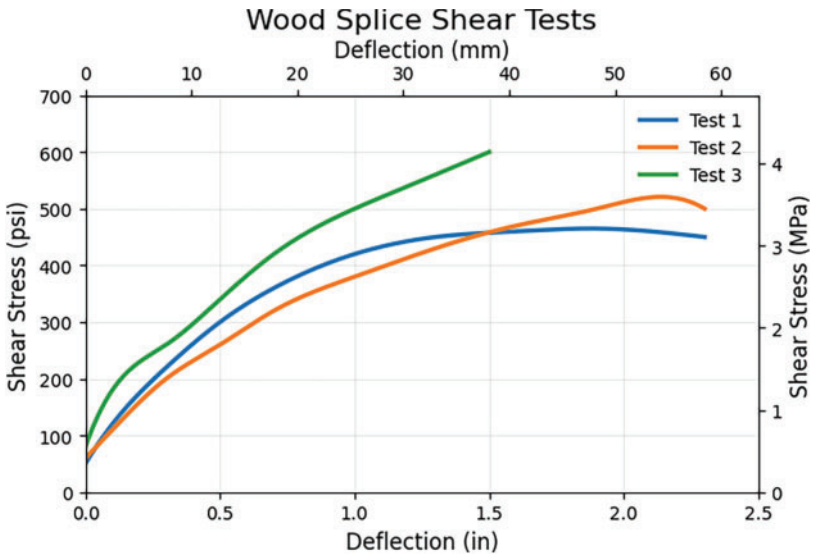

Figure 12. Shear stress versus deflection for wood splice

Table 2. Maximum shear stress and corresponding deflection*

Flat steel plate splicing				
Test	**1**	**2**	**3**	**AVG**
Maximum shear stress (psi; MPa)	614 (4.23)	701 (4.83)	452 (3.12)	589 (4.06)
Deflection at maximum stress (mm)	2.4 (61.0)	3.1 (78.7)	2.5 (63.5)	2.7 (68.6)
Steel C-channel splicing				
Test	**1**	**2**	**3**	**AVG**
Maximum shear stress (psi; MPa)	715 (4.93)	761 (5.25)	873 (6.02)	783 (5.40)
Deflection at maximum stress (mm)	2.3 (58.4)	2.3 (58.4)	2.0 (50.8)	2.2 (55.9)
Wooden plate splicing				
Test	**1**	**2**	**3**	**AVG**
Maximum shear stress (psi; MPa)	484 (3.34)	528 (3.64)	610 (4.21)	541 (3.73)
Deflection at maximum stress (mm)	1.7 (43.2)	2.1 (53.3)	1.5 (38.1)	1.8 (45.7)

*Note: Deflections shown here were recorded at the point of maximum shear stress (not at rupture).
AVG, average.

plate (approximately 2.2 times higher flexural inertia as reported in the Appendix), which is consistent with its improved load-carrying performance observed in the tests. This enhancement is primarily attributed to the three-dimensional geometry, which distributes material farther from the neutral axis. For the FRP-wrapped splice, load transfer is achieved through distributed interface bonding and confinement rather than discrete mechanical connections. This results in a more uniform stress transfer along the splice region and reduced stress concentrations compared to bolted systems. One C-channel specimen was excluded due to instrumentation issues resulting in incomplete data. For the steel plate splice, one specimen exceeded the LVDT measurement range, and the recorded deflection does not represent the true deformation at maximum load.

Data Analysis under Axial Loads

Axial stress versus deflection plots are analyzed using Eqs. (1) and (4) to determine the normal stress for each test specimen, as follows:

$$\sigma = \frac{F}{A} \tag{4}$$

where σ is the axial stress, F is the applied load, and A is the area of cross section.

The axial load testing was performed on three 5 ft (1.52 m) long piles using the three repair methods. Table 4 shows the maximum axial stress and the corresponding deflection. Splice contribution in axial stress computations was not included for simplicity in calculations.

Table 3. Maximum bending stress and corresponding deflection*

Flat steel plate splicing				
Test	**1**	**2**	**3**	**AVG**
Maximum modulus of rupture (psi; MPa)	6674 (46.02)	3647 (25.15)	3417 (23.56)	3532 (24.35)
Deflection at maximum stress (mm)	3.6 (91.4)*	9.5 (241.3)	10.6 (269.2)	10.1 (256.5)
Steel C-channel splicing				
Test	**1**	**2**	**3**	**AVG**
Maximum modulus of rupture (psi; MPa)	2826 (19.48)	4731 (32.62)	Bad Sample	3778 (26.05)
Deflection at maximum stress (mm)	10.2 (259.1)	9.0 (228.6)		9.6 (243.8)
Wooden plate splicing				
Test	**1**	**2**	**3**	**AVG**
Maximum modulus of rupture (psi; MPa)	4609 (31.78)	4860 (33.51)	2415 (16.65)	3962 (27.32)
Deflection at maximum stress (mm)	6.3 (160.0)	7.6 (193.0)	5.4 (137.2)	6.5 (165.1)

*Note: Deflections shown here were recorded at maximum bending stress. Deflection for Test 1 was recorded using LVDT and deflection was maxed at 3.6 in. (91.4 mm); hence, it does not represent deflection at maximum stress.
AVG, average; LVDT, linear variable differential transformer.

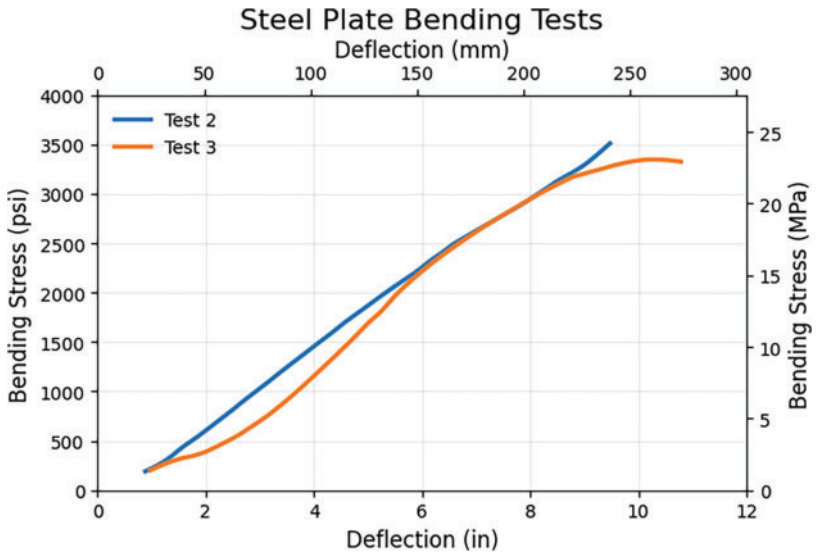

Figure 13. Bending stress versus deflection for steel plate splice

Fig. 16 shows the axial stress versus deflection relationship for specimens with flat steel plate splicing. Piles did not have perfectly flush cuts at the ends where they were in contact with steel plates at each end of the pile. There was an initial loading period of each test when the pile settled into the stiff steel plates that were exerting axial stress at the ends of the cut section of timber piles. Due to this initial settling period, initial axial deflection was nonlinear with applied load by a small amount and was evident in Fig. 17.

Fig. 17 provides the axial stress versus deflection relationship for piles spliced with the steel C-channel splice. Table 4 reveals that the C-channel splice was stronger than that of the flat steel plate splice method in resisting axial compressive loading, which induced a small amount of bending due to eccentricity of applied loads with reference to the geometric centroid of the test specimen.

Fig. 18 provides the axial stress versus deflection relationship for piles spliced with wood plates. Two of the three test specimens provided large deformations at failure. This was attributed to possible "looseness" of the splicing mechanism with the pile, along with a gap separating the portions of the pile at the splice location.

It was apparent that steel plate splicing method was the weakest to transfer axial forces because of its low bending resistance when compared to the other splice mechanisms. The C-channel method was the strongest, since it has the

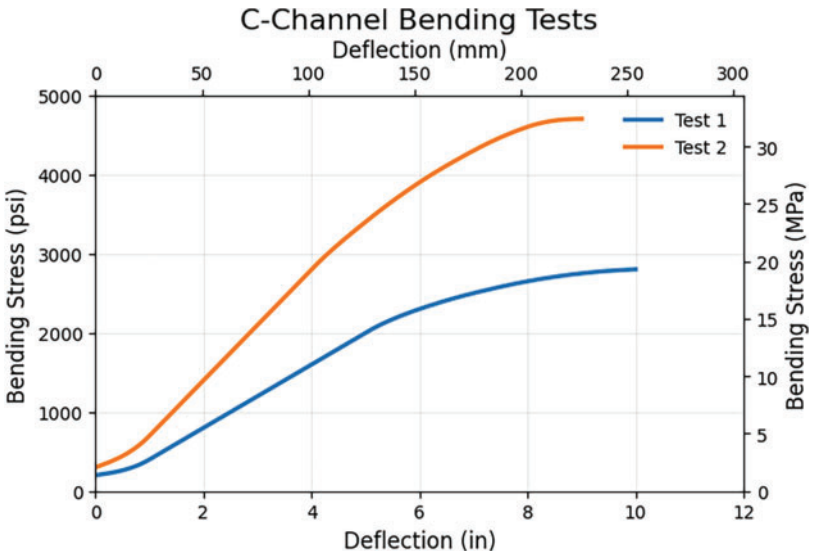

Figure 14. Bending stress versus deflection for C-channel splice

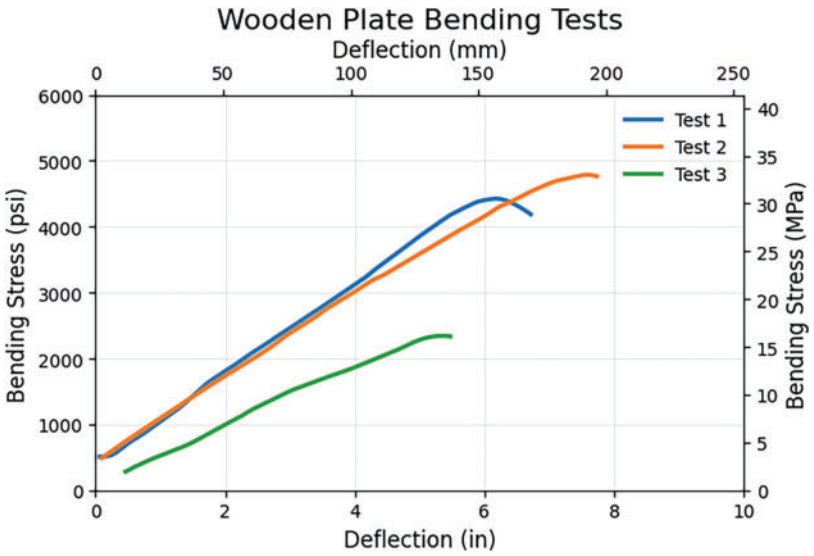

Figure 15. Bending stress versus deflection for wood splicing

highest bending rigidity when compared to the other two splice mechanisms.

A common visual failure observed in majority of the tests was the radial cracking of the pile cross section at both ends where the pile was in contact with the steel plates.

Test Results and Data Analysis for FRP Splicing

Data analysis of FRP splicing under shear

Three FRP-wrapped timber piles were tested under shear to determine the maximum shear stress and the corresponding deflection. Table 5 shows the maximum shear stress and the corresponding deflection for each of the three FRP-spliced specimens, while Fig. 19 provides the shear stress versus deflection plots.

Table 5 reveals lower deflection values at maximum shear stress resistance for the FRP splicing method when compared to the traditional splicing methods. FRP wrap completely confines pile specimens, covering the entire circumference of the spliced area. It also bonds to the timber pile, creating a full shear transfer without slip between the splice mechanism and the good quality portion of a timber pile. As shown in Table 5, maximum shear stress that the FRP-spliced piles can resist is comparable in magnitude to that of the steel plate splicing method.

Failure modes in shear for FRP splicing

FRP splicing ruptures longitudinally near the neutral axis of the pile with the FRP wrap splitting between fibers (Fig. 20), because maximum shear stress is induced under bending at the mid-depth of the test specimens. Furthermore, the failure mode revealed the hoop direction fabric failure,

Table 4. Maximum axial stress and corresponding deflection*

Flat steel plate splicing				
Test	**1**	**2**	**3**	**AVG**
Maximum axial stress (psi; MPa)	1038 (7.16)	856 (5.90)	831 (5.73)	909 (6.27)
Deflection at maximum stress (mm)	0.4 (10.2)	0.7 (17.8)	0.5 (12.7)	0.5 (12.7)
Steel C-channel splicing				
Test	**1**	**2**	**3**	**AVG**
Maximum axial stress (psi; MPa)	2214 (15.26)	1423 (9.81)	1412 (9.74)	1683 (11.60)
Deflection at maximum stress (mm)	0.5 (12.7)	0.6 (15.2)	0.6 (15.2)	0.6 (15.2)
Wooden plate splicing				
Test	**1**	**2**	**3**	**AVG**
Maximum axial stress (psi; MPa)	1492 (10.29)	1494 (10.30)	1709 (11.78)	1565 (10.79)
Deflection at maximum stress (mm)	0.6 (15.2)	1.1 (27.9)	0.3 (7.6)	0.6 (15.2)

*Note: Deflections were identified at the point of maximum axial stress.
AVG, average.

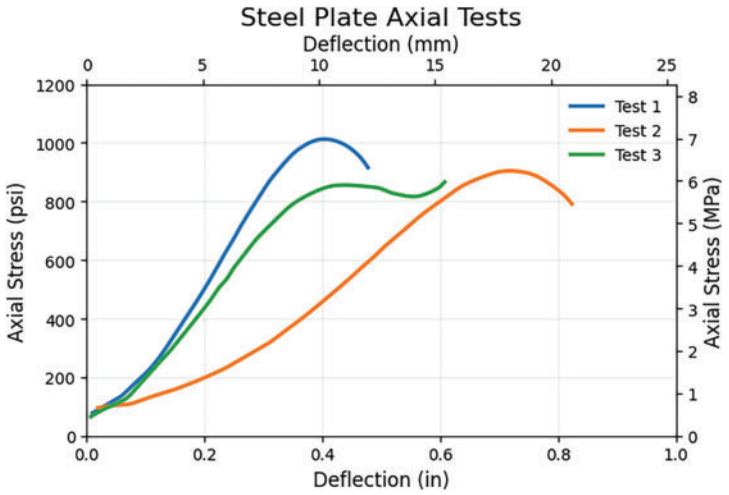

Figure 16. Axial stress versus deflection for flat steel plate splice

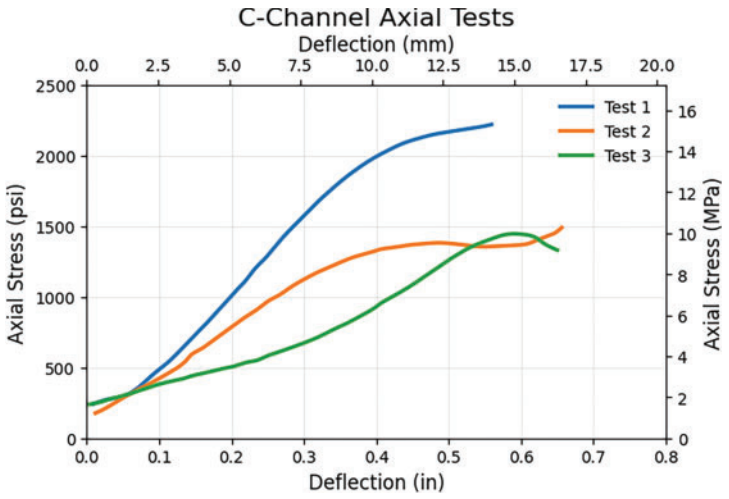

Figure 17. Axial stress versus deflection for C-channel splice

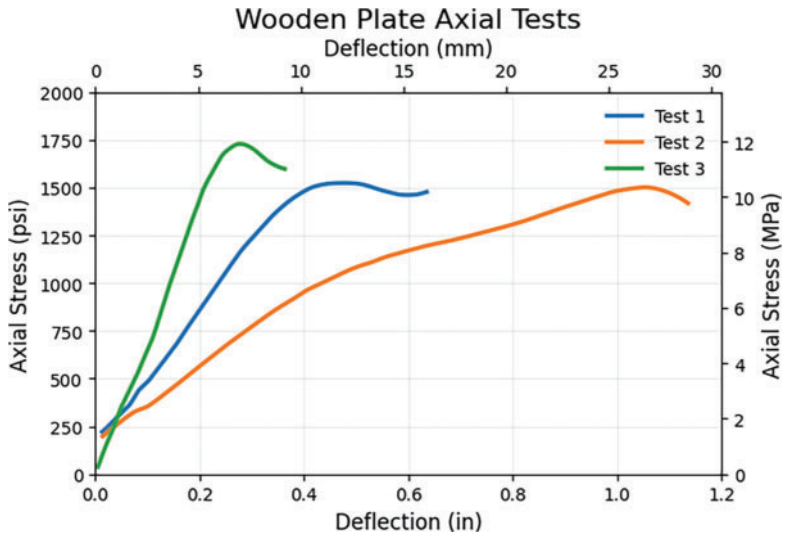

Figure 18. Axial stress versus deflection for wood splice

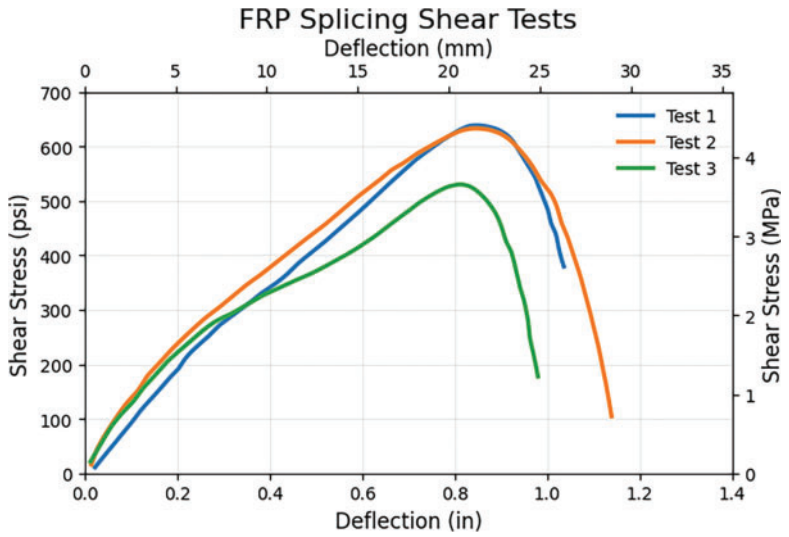

Figure 19. Shear stress versus deflection with FRP splice. FRP, fiber-reinforced polymer

Table 5. FRP splice maximum shear and corresponding deflection

Test	1	2	3	AVG
Maximum shear stress (psi; MPa)	657 (4.53)	643 (4.43)	539 (3.72)	613 (4.23)
Deflection at maximum stress (mm)	0.9 (22.9)	0.9 (22.9)	0.9 (22.9)	0.9 (22.9)

Note: AVG, average; FRP, FRP, fiber-reinforced polymer.

where hoop fiber was minimal. Therefore, shear resistance of FRP-spliced piles can be improved by modifying the fiber architecture. During loading and unloading stages, buckling related deformation was observed in the splice as shown in Fig. 20.

Data analysis of FRP-spliced pile under bending testing

The bending test data were analyzed for maximum bending stress versus deflection as given in Table 6. Fig. 21 provides the bending stress versus deflection plots for piles spliced with FRP wraps, revealing lower deflection as well as maximum stress than the traditional methods of splicing. This indicates that not enough reinforcement was provided through the FRP wrap for adequate resistance to bending stress. The "dips" in Tests 2 and 3 in the bending stress versus deflection plots (Fig. 21) are an indication of local buckling and/or debonding of wrap under low bending induced stresses, which is elaborated below.

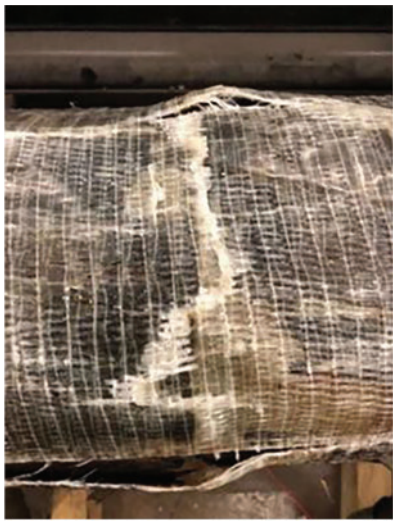

Figure 20. FRP splice cracking under applied load at top

Discussion of failure modes in bending for FRP splicing

Lack of adequate quantity of fibers in the hoop direction caused the FRP to "unzip" along its length with increasing deformation. This deficiency could be remedied easily by adding extra layers of fibers in the hoop direction of glass fabric layers. As in shear testing, ultimate failure happened rapidly and occurred between fibers in the longitudinal direction, indicating failure in hoop fibers. Under bending, large portions of FRP fabric debonded from the pile (Fig. 22). In one of the specimens, a different form of failure was observed, as shown in Fig. 23. The splice failed at the center in the form of fiber splitting, further indicating the inadequacy of glass fiber content.

The failure mechanisms observed in the FRP-spliced specimens can be interpreted based on established mechanics of confined and bonded composite systems. Under bending, the FRP wrap is subjected to tensile stresses in the longitudinal direction and shear stresses at the interface between the composite and timber substrate. When the hoop reinforcement is insufficient, the lateral confinement effect is reduced, leading to increased tensile strain concentration and premature longitudinal splitting (unzipping) of fibers. The observed debonding and local buckling behavior can be associated with interface shear stress exceeding the bond capacity between the FRP and timber. In such cases, partial loss of composite action occurs, resulting in nonuniform stress transfer and increased deformation variability. This behavior consists of bond slip mechanisms commonly observed in FRP-strengthened structural members. Under axial loading, the FRP wrap provides confinement to the timber core, generating lateral pressure that enhances load-carrying capacity. However, the presence of gaps or discontinuities at the splice location can lead to localized stress concentrations, causing bulging and subsequent splitting of fibers in the hoop direction. This indicates that interface integrity and confinement effectiveness are critical in governing the structural response.

Analysis of FRP splicing under axial testing

The purpose of the axial test was to determine the maximum axial stress and its corresponding deflection for each of the three FRP-spliced timber specimens tested herein. Table 7 shows the maximum axial stress versus deflection for each of the three FRP-spliced specimens and also the average maximum axial stress and average axial deflection. Fig. 24 shows axial stress versus deflection for piles spliced using FRP wrap. FRP splicing provides a significant increase in strength under axial compression when compared with traditional splicing methods. The FRP splicing under axial loading was the strongest out of all the methods of splicing studied herein, i.e., 1753 psi (12.09 MPa) versus 1683 psi (11.6 MPa).

Discussion of FRP splicing failure modes under axial load

Due to the gap between the two halves of a pile specimen, bulging of fiber in the FRP wrap at the center was noticed. This occurred in each of the three specimens tested. Adding a layer of high-strength caulking in the gap between pile halves can prevent bulging by minimizing localized stress concentration. In this test, bulging fibers were split in the hoop direction but remained intact in the longitudinal direction along the pile (Fig. 25). This bulging in all three test specimens indicates that buckling followed by debonding of the FRP wrap at the center of the splice.

In summary, splicing of timber piles with FRP wraps provides structural performance comparable to traditional splicing methods, especially in terms of axial and shear stresses. Bending stress resistance, however, was not as high as anticipated, which could be improved easily by adding extra layers of fabric in the hoop direction of fibers, but not very critical for piles since 90% of the load acts in the axial direction. Table 8 summarizes the test data of the FRP wrap repair specimens and traditional splicing methods under different loads.

Table 6. FRP splice maximum MOR and corresponding deflection

Test	1	2	3	AVG
Maximum modulus of rupture (psi; MPa)	2032 (14.01)	2402 (16.56)	2129 (14.68)	2188 (15.09)
Deflection at maximum stress (mm)	2.3 (58.4)	3.5 (88.9)	5.1 (129.5)	3.6 (91.4)

Note: AVG, average; FRP, FRP, fiber-reinforced polymer; MOR, modulus of rupture.

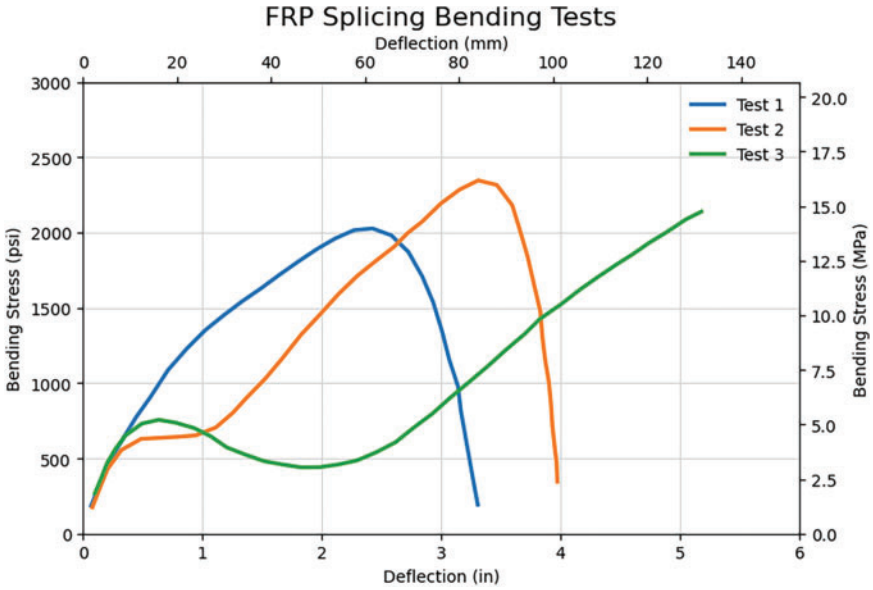

Figure 21. Bending stress versus deflection with FRP splice. FRP, fiber-reinforced polymer

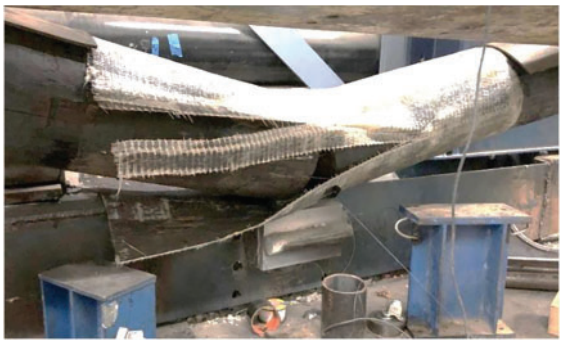

Figure 22. Debonding of splice at failure under bending

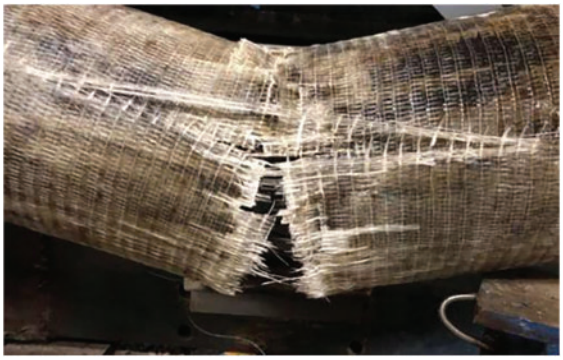

Figure 23. FRP splice failure at center under bending. FRP, fiber-reinforced polymer

Improved FRP Splice Design and Durability

Bending capacities of FRP wrap splicing were lower than those of the traditional splicing methods. To improve the load resistance under bending, a modified design was developed, that is, a six-layer, bidirectional FRP wrap design. Three additional layers of FRP wrap were added to the original splice design, using unidirectional Sika fabric (dry density of 0.092 lb/in^3 (2547.0 kg/m^3)), with fiber orientation of three layers each in the hoop and longitudinal directions of a pile.

For the six-layer FRP wrap design, one shear and two bending tests were performed in the same manner as described above. A pile with the three-layer unidirectional fabric design that was taken to failure under four-point bending was repaired using three additional virgin layers of fabric, with the strength-dominant fiber direction aligned with the hoop direction of the pile. This repaired specimen with six layers was retested under four-point bending load condition.

Shear analysis with improved FRP wrap

The shear stress versus deflection from the six-layer shear test is shown in Fig. 26, and maximum values are found to be 987 psi (6.81 MPa) and 2.0 in. (50.8 mm), respectively. This splice performed better than the three traditional splicing methods and also the three-layer FRP splice. Fig. 26 revealed that the shear stress leveled off after about 0.9 in. (22.9 mm) of deflection, which is identical to deflection of three-layer wrap case. This could be due to internal pile failure, and test pile was not able to resist stress beyond 987 psi (6.81 MPa). It is interesting to note that the deflection of the pile spliced with six layers of FRP was only 0.51 in. (13.0 mm) at 613 psi (4.23 MPa), whereas 0.9 in. (22.9 mm) was the deflection for three-layered FRP-wrapped system at 613 psi (4.23 MPa) stress. The failure mode (Fig. 26) was ductile in the six-layer FRP wrap specimen, and the failure occurred in compression at the center of the splice (Fig. 27) with no zipping.

Bending analysis with improved FRP wrap

The six-layered wrap-spliced pile was tested under four-point bending in the same manner as discussed earlier, and failure modes are consistent with those presented for the three-layer wrap piles. The rewrapped piles with additional three

Table 7. FRP splice maximum axial stress and corresponding deflection

Test	1	2	3	AVG
Maximum axial stress (psi; MPa)	1339 (9.23)	1776 (12.25)	2143 (14.78)	1753 (12.09)
Deflection at maximum stress (mm)	0.5 (12.7)	0.6 (15.2)	0.7 (17.8)	0.6 (15.2)

Note: AVG, average; FRP, FRP, fiber-reinforced polymer.

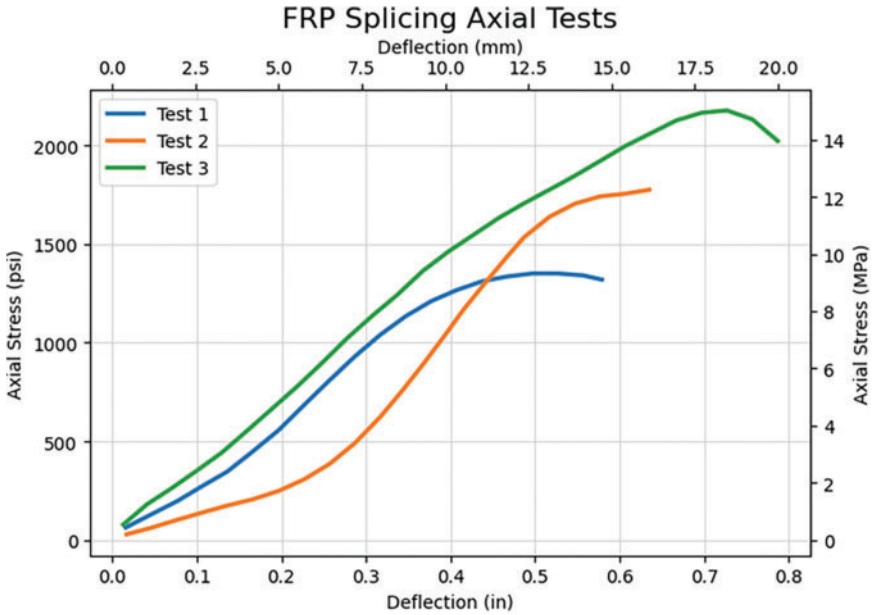

Figure 24. Axial stress versus deflection for FRP splice. FRP, fiber-reinforced polymer

Figure 25. Bulging in FRP splice under compression. FRP, fiber-reinforced polymer

layer (total 6 layers) recorded a lower failure bending stress (2321 versus 2974 psi) and higher deflection (5.0 versus 2.7 in.). The maximum bending stress recorded in the rewrapped pile test is similar to the maximum bending stress recorded from the test data of the pristine three-layer FRP wrap-spliced pile.

Bending stress versus deflection plots for the repaired or rewrapped pile as well as the six-layer pristine specimen are shown in Fig. 28. The stiffness of rewrapped specimen was lower than that of the pristine three-wrap FRP-spliced specimens due to inadequate bending transfer across the failed joint of the pristine three-wrap system. Large deflections from this test are attributed to already failed original splice with three-layered FRP wrap. With the three bottom layers having already failed, significant debonding between the splice mechanism and the pile is observed, resulting in larger deflections. Therefore, the bending capacity of the rewrapped systems is developed from the three additional (new) layers of fabric after initial testing to failure with three layers, and not six layers including original three layers.

The overall strength and stiffness of the six-layer wrapped pristine pile were higher than that of the original three-layer FRP wrap test specimens (Table 9). Performance of the rewrapped (already failed and repaired) specimen provided a slight increase (6%) in bending stress capacity from the original design, providing larger deflection at ultimate stress. Results from the pristine six-layer spliced pile revealed that additional layers of wrap do help in increasing the strength capacity of the system by about 36%. The main failure mode was the debonding of layers and buckling of the FRP splice. The pristine pile with six layers of FRP showed a 61% increase in shear stress to failure from the original three-layer design. A comparison of the bending data of the pristine six-layer FRP splice design and the original three-layer FRP splice design revealed that the six-layer design under bending provides a 36% increase in bending load to failure.

Maximum bending stress, recorded in the four-point bending test of the virgin timber pile, exceeded the maximum bending stress for each of the splicing methods previously

Table 8. Average maximum stress and deflection for all splice methods

Method of splicing	Steel plate	C-channel	Wooden plate	FRP (three layer) wrap
Shear stress (psi, MPa)	589 (4.06)	783 (5.40)	541 (3.73)	613 (4.23)
Deflection in shear (mm)	2.7 (68.6)	2.2 (55.9)	1.8 (45.7)	0.9 (22.9)
Modulus of rupture (psi; MPa)	3532 (24.35)	3778 (26.05)	3962 (27.32)	2188 (15.09)
Deflection in bending (mm)	10.1 (256.5)	9.6 (243.8)	6.5 (165.1)	3.6 (91.4)
Axial stress (psi; MPa)	909 (6.27)	1683 (11.60)	1565 (10.79)	1753 (12.09)
Deflection in axial (mm)	0.5 (12.7)	0.6 (15.2)	0.6 (15.2)	0.6 (15.2)

Note: FRP, fiber-reinforced polymer.

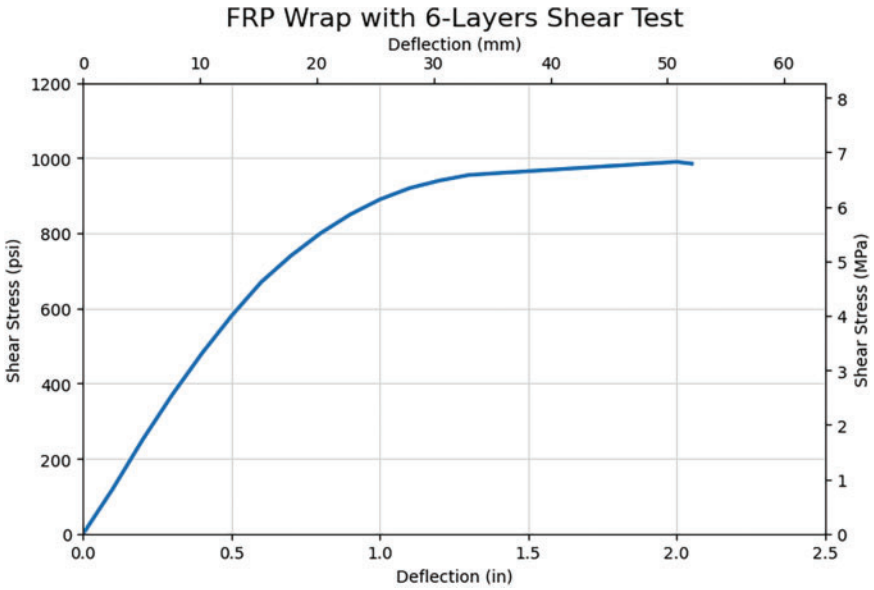

Figure 26. Six-layer FRP shear stress versus deflection. FRP, fiber-reinforced polymer

Figure 27. Compressive failure of fabric

discussed. Table 8 provides a comparison of the maximum stress and corresponding deflection for the virgin timber pile and various splicing methods, proving that splicing a pile creates a certain reduction in the pile bending strength. The addition of GFRP fabrics in splicing mechanisms to a pile system greatly increases the bending deflection recorded at maximum bending stress. Traditional splicing methods provide much higher deflection than the virgin pile, which is attributed to excess lateral movement under bending due to inadequate restraint of pile sections.

The durability response of any structural system is a function of physical, chemical, and mechanical aging under variations in moisture, temperature, pH, fatigue and ultraviolet radiation. Based on earlier field studies dealing with repair and rehabilitation of wood bridge piles (18 and 20) in service since the year 2000 on South Branch Valley Rail-WVDOT, no delamination of FRP wrap from timber substrate was detected. Any potential delamination can be fixed by injecting resin into the voids through the existing FRP wraps. Practical suggestions of in situ fixing of debonded spots were suggested by ACI 440-13-24. Statistical analysis of the experimental data could not be performed because: 1) the data are very limited in terms of replications (1 or 2); 2) large-size timbers exhibit high variability in mechanical properties, as evident from the data generated herein; and 3) many independent material and rehabilitation

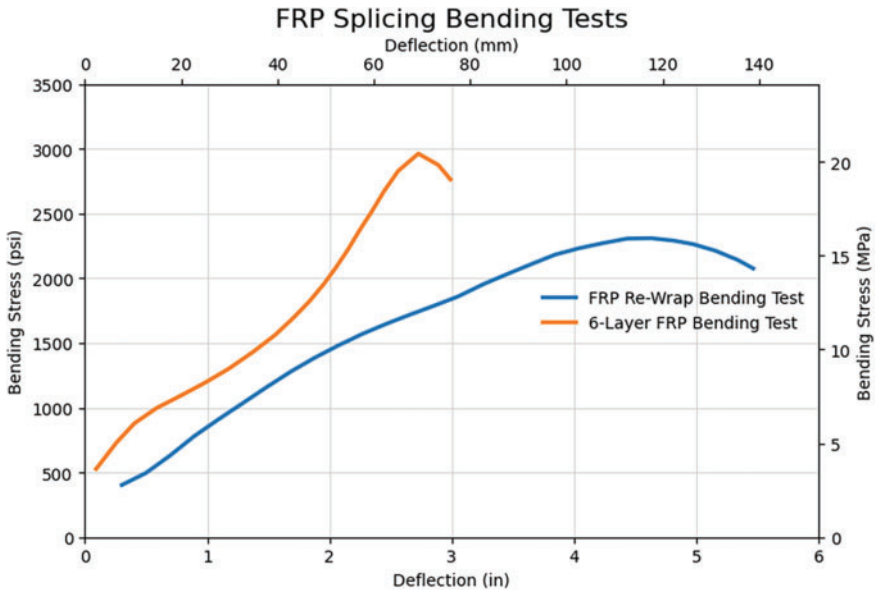

Figure 28. FRP rewrap bending stress versus deflection. FRP, fiber-reinforced polymer

Table 9. Comparison of bending stress and deflection between virgin pile and spliced piles

Splice mechanism	Virgin pile	Steel plate	C-channel	Wood plate	FRP (Three-Layer)	FRP (Six-layer rewrap)	FRP (Six-layer pristine)
Maximum modulus of rupture (psi; MPa)	5714 (39.40)	3532 (24.35)	3778 (26.05)	3962 (27.32)	2188 (15.09)	2321 (16.00)	2974 (20.51)
Deflection at maximum stress (mm)	3.2 (81.3)	10.1 (256.5)	9.6 (243.8)	6.5 (165.1)	3.6 (91.4)	5.0 (127.0)	2.7 (68.6)
Percent stress loss (%)	–	38.2	33.9	30.7	61.7	59.4	47.9

Note: FRP, fiber-reinforced polymer.

parameters were not controlled, limiting the ability to obtain meaningful analysis.

Conclusions

- Based on both the laboratory and field experiences, traditional splicing methods are more cumbersome to rehabilitate than FRP wrapping techniques.
- Traditional splicing methods cause larger movement in the pile system under loading due to bolted splice mechanism; however, FRP wrap splicing has no relative movement between the two spliced sections under loading due to full bond between the wrap and the two timber substrate (pile) spliced together.
- Three-layer unidirectional FRP wrap-spliced piles performed better under axial loading than the traditional methods.
- Three-layer unidirectional FRP wrap-spliced piles failed under bending by unzipping of the fabric between orthogonal fibers, i.e., additional reinforcement is essential in the hoop direction to prevent such failure modes.
- Adding three additional fabric layers (six layers in total) to reinforce the hoop direction, improved the shear stress capacity by 61% and the bending capacity by 36% compared to the three-layer FRP splice design. The shear capacity of six-layer FRP splice design exceeded the shear capacity of all three traditional splicing methods, where the bending capacity of six-layer FRP wrap was still lower than the three traditional methods, which can be improved by adding extra layers of fibers in the longitudinal (bending) direction.
- Splicing a timber pile with mechanical splice mechanisms tested in this program decreases the bending capacity in relation to uncut continuous timber pile system.
- Traditional splicing methods may be more costly than FRP wrap splicing techniques, considering factors such as material weight, transportation, and labor requirements as elaborated by Damich;[23–26] however, a detailed cost analysis was not performed in this study.

Acknowledegments

We would like to express our gratitude to Louisiana Transportation Research Center (LTRC) and the Louisiana Transportation Research Center (LDOT) for the financial support of this research activity. Also, we are grateful to Stella-Jones for providing full-size treated timber piles to conduct testing.

Data Availability Statement

The data that support the findings of this study are available from the corresponding author upon request.

References

[1] Eslyn W, Clark J. *Wood Bridges-Decay Inspection and Control*. Madison: Agricultural Handbook NO. 557; 1979.

[2] Duwadi SR, Ritter M. Timber bridges in the United States. *Public Roads*. 1997;60(3):32–40. doi:10.2749/222137801796348629.

[3] Pilejax. Rapid repair systems—timber pile repair. http://www.joinlox.com/wp-content/uploads/2016/07/PILEJAX_Timber-WhitePaper_FINAL_TW.pdf.

[4] Barrow RS. Fuzzy wood and coastal piles. *Struct Mag*. 2023:20–21. https://www.structuremag.org/article/fuzzy-wood-and-coastal-piles/.

[5] Zelada-Tumialan GA, Konicki W, Westover P, Vatovec M. Untreated submerged timber pile foundations: Part 1–understanding biodegradation and compressive strength. *Struct Mag*. 2013:9–11. https://www.structuremag.org/article/untreated-submerged-timber-pile-foundations-part-1-understanding-biodegradation-and-compressive-strength/.

[6] MnDOT. Bridge inspection for decay and other deterioration. In: *Timber Bridges: Design, Construction, Inspection, and Maintenance*. 1990:13.

[7] Substructure.com. Wood structures are subject to various types of damage in the marine environment, mostly biological; 2015. https://www.substructure.com/about/marine-services-information/marine-corrosion/wood-corrosion.

[8] Azizinamini A, Mohammadi A, Gull J, Taghinezhad R. Assessment and evaluation of timber piles used in Nebraska for retrofit and rating. *Nebraska Depart Transport Res*. 2014. doi:10.3141/2481-16.

[9] Dahlberg J, Phares B, Klaiber W. Cost-effective timber bridge repairs: manual for repairs of timber bridges in Minnesota. Minnesota Department of Transportation. 2015;MN/RC 2015-45B. https://bec.iastate.edu/wp-content/uploads/2018/03/201545B.pdf.

[10] Dahlberg J, Phares B, Bigelow J, Klaiber FW. Timber abutment piling and back wall rehabilitation and repair. Bridge Engineering Center, Iowa State University. 2012;TR-616. https://www.intrans.iastate.edu/wp-content/uploads/2018/03/tr-616_timber_abut_w_cvr.pdf.

[11] Klaiber FW, White DJ, Wipf TJ, Mekkaway M, Koskie J. Investigation of steel stringer bridges: superstructures and substructures. *Bridge Eng Center*. 2007. doi:10.31274/rtd-180813-16540.

[12] Wipf TJ, Fanous FS, Klaiber FW, Eapen AS. Evaluation of appropriate maintenance, repair and rehabilitation methods for Iowa bridges. Iowa State University, Department of Civil Engineering. 2003;TR-429. https://rosap.ntl.bts.gov/view/dot/39501.

[13] GangaRao H, Kenney A, Zhang C, Bhandari L, Liang R. Mechanical response of glass/kevlar hybrid composite jackets for steel containers carrying hazardous materials to enhance safety. *Sustain Struct*. 2024;4(3). doi:10.54113/j.sust.2024.000055.

[14] Zhang C, Tan KT. Low-velocity impact response and compression after impact behavior of tubular composite sandwich structures. *Compos Part B: Eng*. 2020;193(12):108026. doi:10.1016/j.compositesb.2020.108026.

[15] Zhang C, Tan KT. Experimental and numerical investigation of large-scale effect on buckling and post-buckling behavior of tubular structures. *Thin-Wall Struct*. 2023;186:110708. doi:10.1016/j.tws.2023.110708.

[16] Mallick PK. *Fiber-Reinforced Composites: Materials, Manufacturing and Design*. Boca Raton: CRC Press, Taylor and Francis Group; 2007.

[17] de la Rosa García P, Escamilla AC, Nieves González García M. Bending reinforcement of timber beams with composite carbon fiber and basalt fiber materials. *Compos Part B: Eng*. 2013;55(4):528–536. ISSN 1359-8368. doi:10.1016/j.compositesb.2013.07.016.

[18] Li L, Yuan S, Dong J, Wang Q. An experimental study on the axial compressive behavior of timber columns strengthened by FRP sheets with different wrapping methods. *Appl Mech Mat*. 2013;351–352:1419–1422. doi:10.4028/www.scientific.net/amm.351-352.1419.

[19] Petro S, GangaRao HVS, Halabe U, et al. *Carbon Fiber Reinforced Polymer Composites Used to Repair and Rehabilitate Wood Railroad Bridges*. Charleston, WV: West Virginia Department of Transportation; 2007.

[20] Smith A. Rehabilitation of timber railroad bridges using glass fiber reinforced polymer composite wraps. Graduate Thesis Dissertations and Problem Reports; 2004. doi:10.33915/etd.1462.

[21] Vijay P, GangaRao H, Liang R, Skidmore M. Rapid restoration of rail raod timber bridges using polymer composites. *ANTEC*. 2011. doi:10.1115/jrc2010-36053.

[22] Alkhrdaji T. Strengthening of concrete structures using FRP composites. *Struct Mag*. 2015 June. https://www.structuremag.org/article/strengthening-of-concrete-structures-using-frp-composites/.

[23] Damich, Drew L. Timber Bridge Pile Splicing with Fiber Reinforced Polymer Wraps. Graduate Theses, Dissertations, and Problem Reports; 2021:8291. https://researchrepository.wvu.edu/etd/8291/https://doi.org/10.33915/etd.8291.

[24] Army and Air Force. *Bridge Inspection, Maintenance, and Repair (TM 5-600/AFJPAM 32-1088)*. Washington, DC: Joint Departments of Army and Air; 1994.

[25] GangaRao HVS, Taly N, Vijay PV. *Reinforced Concrete Design With FRP Composites*. Boca Raton: CRC Press, Taylor and Francis Group; 2007.

[26] ASTM International. *ASTM D7565: Standard Test Method for Determining Tensile Properties of Fiber Reinforced Polymer Matrix Composites Used for Strengthening of Civil Structures*. West Conshohocken, PA: ASTM; 2017.

Appendix: Statistical Summary and Simplified Mechanical Analysis of Splice Systems

To provide additional insight into the variability of the experimental data, statistical descriptors including standard deviation and coefficient of variation (COV) were calculated for all test configurations. These metrics are presented to supplement the average values reported in the main manuscript.

The variability of shear strength among specimens was quantified using the coefficient of variation (COV), which ranged from approximately 10% to 22% for traditional splice systems. The steel plate splice exhibited the highest variability, whereas the C-channel splice showed both higher strength and lower variability, indicating more consistent performance. In comparison, the FRP splice demonstrated relatively low variability in shear strength (COV $\approx$ 10%) and highly consistent deformation behavior.

The bending test results exhibited relatively high variability, with coefficients of variation (COV) ranging from approximately 34% to 40% for traditional splice systems. This variability is attributed to the inherent heterogeneity of timber materials and differences in failure modes among specimens. Therefore, caution should be exercised when directly comparing splice configurations based solely on average bending strength.

The variability of axial stress ranged from approximately 8% to 27% across all splice configurations, indicating moderate consistency among specimens. The C-channel splice demonstrated higher axial strength among traditional methods, while the FRP splice exhibited the highest overall axial capacity.

Although the FRP splice showed moderate variability in strength (coefficients of variation [COV] $\approx$ 23%), the deformation response remained relatively consistent, suggesting stable load transfer under axial compression.

Based on the splice geometry above, a simplified section-property comparison was performed. The flat steel plate can be approximated as a rectangular section (6 in. $\times$ 0.5 in.), resulting in a second moment of area $I \approx 9.0\,\text{in.}^4$ and a section modulus $S \approx 3.0\,\text{in.}^3$. In contrast, the C-channel, with a nominal depth of 8 in and flange/web configuration, yields an approximate $I \approx 19.6\text{in.}^4$ and $S \approx 4.9\,\text{in.}^3$. This indicates that the C-channel provides approximately 2.2 times the flexural inertia and 1.6 times the section modulus compared to the flat plate. The increased stiffness and section modulus, resulting from the three-dimensional geometry and material distribution away from the neutral axis, contribute to the improved load-carrying performance of the steel C-channel splice. It should be noted that this comparison is based on idealized section properties and does not account for bolt slip, local bearing, or composite interaction with timber.

The load transfer mechanism in the FRP-wrapped splice can be interpreted in terms of interface bonding and confinement effects. Unlike mechanically fastened steel splices, where load transfer is primarily achieved through discrete bolt connections, the FRP wrap enables a more distributed transfer of force along the bonded interface. In a simplified form, the average interfacial shear stress may be expressed as

$$\tau_{avg} = \frac{T}{\pi d L_e}$$

where T is the transferred force, d is the effective diameter of the wrapped section, and L_e is the effective bond length which is less than the actual wrap length due to nonlinear force transfer along the wrap length and it is estimated to be around 40% of actual bond length. L_e can be accurately determined after conducting several inter facial shear tests. This relationship indicates that, for a given transferred force, a larger bonded perimeter and longer development length reduce the average interface shear demand and promote a more uniform transfer of load. Therefore, compared with bolted splices that introduce localized force transfer and stress concentrations, the bonded FRP wrap is expected to provide a more continuous stress transfer path.

Table A1. Maximum shear stress and corresponding deflection*

Flat Steel Plate Splicing					
Test	1	2	3	AVG	Mean ± SD (COV %)
Maximum Shear Stress (psi)	614	701	452	589	589 ± 126 (21.5%)
Deflection at Maximum Stress (in.)	2.4	3.1	2.5	2.7	2.67 ± 0.38 (14.2%)
Steel C-Channel Splicing					
Test	1	2	3	AVG	Mean ± SD (COV %)
Maximum Shear Stress (psi)	715	761	873	783	783 ± 81 (10.4%)
Deflection at Maximum Stress (in.)	2.3	2.3	2	2.2	2.20 ± 0.17 (7.9%)
Wooden Plate Splicing					
Test	1	2	3	AVG	Mean ± SD (COV %)
Maximum Shear Stress (psi)	484	528	610	541	541 ± 64 (11.8%)
Deflection at Maximum Stress (in.)	1.7	2.1	1.5	1.8	1.77 ± 0.31 (17.3%)

Note: AVG, average; COV, coefficients of variation; FRP, fiber-reinforced polymer; SD, standard deviation.

Table A2. Maximum bending stress and corresponding deflection*

Flat steel plate splicing					
Test	1	2	3	AVG	Mean ± SD (COV %)
Maximum modulus of rupture (psi)	6674	3647	3417	4579.3	3532 ± 163 (4.6%)
Deflection at maximum stress (in.)	3.6*	9.5	10.6	7.9	10.05 ± 0.78 (7.8%)
Steel C-channel splicing					
Test	1	2		AVG	Mean ± SD (COV %)
Maximum modulus of rupture (psi)	2826	4731		3778.5	3778 ± 1347 (35.6%)
Deflection at maximum stress (in.)	10.2	9		9.6	9.60 ± 0.85 (8.8%)
Wooden plate splicing					
Test	1	2	3	AVG	Mean ± SD (COV %)
Maximum modulus of rupture (psi)	4609	4860	2415	3961.3	3961 ± 1345 (34.0%)
Deflection at maximum stress (in.)	6.3	7.6	5.4	6.4	6.43 ± 1.11 (17.2%)

Note: AVG, average; COV, coefficients of variation; SD, standard deviation.

Table A3. Maximum axial stress and corresponding deflection*

Test	1	2	3	AVG	Mean ± SD (COV %)
Maximum axial stress (psi)	1038	856	831	909	908 ± 113 (12.4%)
Deflection at maximum stress (in.)	0.4	0.7	0.5	0.5	0.53 ± 0.15 (28.6%)
Steel C-channel splicing					
Test	1	2	3	AVG	Mean ± SD (COV %)
Maximum axial stress (psi)	2214	1423	1412	1683	1683 ± 460 (27.3%)
Deflection at maximum stress (in.)	0.5	0.6	0.6	0.6	0.57 ± 0.06 (10.2%)
Wooden plate splicing					
Test	1	2	3	AVG	Mean ± SD (COV %)
Maximum axial stress (psi)	1492	1494	1709	1565	1565 ± 125 (8.0%)
Deflection at maximum stress (in.)	0.6	1.1	0.3	0.6	0.67 ± 0.40 (60.6%)

Note: AVG, average; COV, coefficients of variation; FRP, fiber-reinforced polymer; SD, standard deviation.

Table A4. FRP splice maximum shear stress and corresponding deflection

Test	1	2	3	AVG	Mean ± SD (COV %)
Maximum shear stress (psi)	657	643	539	613	613 ± 64 (10.5%)
Deflection at maximum stress (in.)	0.9	0.9	0.9	0.9	0.90 ± 0.00 (0.0%)

Note: AVG, average; COV, coefficients of variation; FRP, fiber-reinforced polymer; SD, standard deviation.

Table A5. FRP splice maximum MOR and corresponding deflection

Test	1	2	3	AVG	Mean ± SD (COV %)
Maximum modulus of rupture (psi)	2032	2402	2129	2188	2188 ± 192 (8.8%)
Deflection at maximum stress (in.)	2.3	3.5	5.1	3.6	3.63 ± 1.40 (38.7%)

Note: AVG, average; COV, coefficients of variation; FRP, fiber-reinforced polymer; MOR, modulus of rupture; SD, standard deviation.

Table A6. FRP splice maximum axial stress and corresponding deflection

Test	1	2	3	AVG	Mean ± SD (COV %)
Maximum axial stress (psi)	1339	1776	2143	1753	1753 ± 403 (23.0%)
Deflection at maximum stress (in.)	0.5	0.6	0.7	0.6	0.60 ± 0.10 (16.7%)

Note: AVG, average; COV, coefficients of variation; FRP, fiber-reinforced polymer; SD, standard deviation.

Table A7. Average maximum stress and deflection for all splice methods

Method of splicing	Steel plate	C-channel	Wooden plate	FRP wrap
Shear stress (psi)	589 ± 126 (21.5%)	783 ± 81 (10.4%)	541 ± 64 (11.8%)	613 ± 64 (10.5%)
Deflection in shear (in.)	2.67 ± 0.38 (14.2%)	2.20 ± 0.17 (7.9%)	1.77 ± 0.31 (17.3%)	0.90 ± 0.00 (0.0%)
Modulus of rupture (psi)	3532 ± 163 (4.6%)*	3778 ± 1347 (35.6%)	3961 ± 1345 (34.0%)	2188 ± 192 (8.8%)
Deflection in bending (in.)	10.05 ± 0.78 (7.8%)*	9.60 ± 0.85 (8.8%)	6.43 ± 1.11 (17.2%)	3.63 ± 1.40 (38.7%)
Axial stress (psi)	908 ± 113 (12.4%)	1683 ± 460 (27.3%)	1565 ± 125 (8.0%)	1753 ± 403 (23.0%)
Deflection in axial (in.)	0.53 ± 0.15 (28.6%)	0.57 ± 0.06 (10.2%)	0.67 ± 0.40 (60.6%)	0.60 ± 0.10 (16.7%)

Note: FRP, fiber-reinforced polymer.

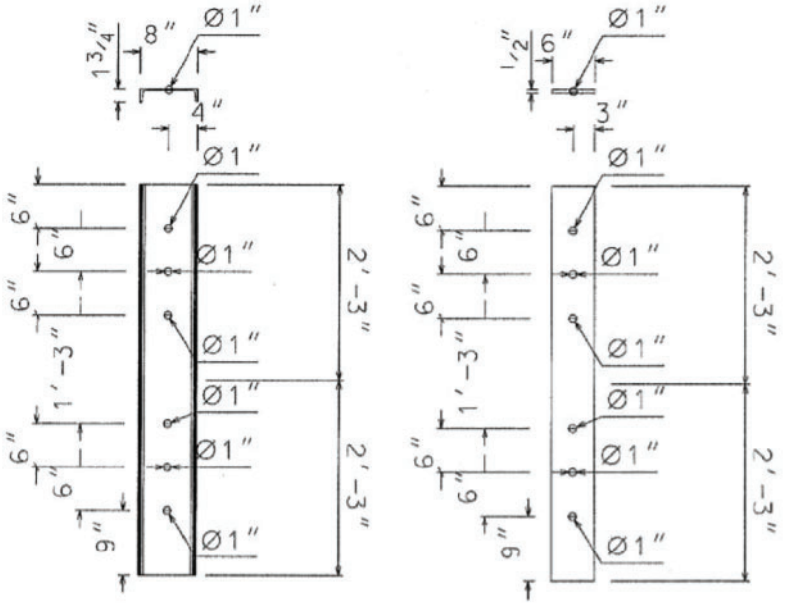

Figure A1. Details of steel plate and c-channel splice configurations